Micro-cracking monitoring and fracture evaluation for crumb rubber concrete based on acoustic emission techniques

Article *in* Structural Health Monitoring · September 2017

DOI: 10.1177/1475921717730538

CITATIONS
5

READS
120

5 authors, including:

Jie Xu
Tianjin University
36 PUBLICATIONS **165** CITATIONS
SEE PROFILE

Giuseppe Lacidogna
Politecnico di Torino
188 PUBLICATIONS **2,466** CITATIONS
SEE PROFILE

Original Article

Structural Health Monitoring
2018, Vol. 17(4) 946–958

DOI: 10.1177/1475921717730538
journals.sagepub.com/home/shm

Micro-cracking monitoring and fracture evaluation for crumb rubber concrete based on acoustic emission techniques

Jie Xu[1], Zhengwu Fu[1], Qinghua Han[1], Giuseppe Lacidogna[2] and Alberto Carpinteri[2]

Abstract

A micro-cracking monitoring and fracture evaluation method for crumb rubber concrete based on the acoustic emission technique was developed. The precursory micro-cracking activity and fracture behavior of crumb rubber concrete with different rubber contents, 0%, 10%, and 15%, were analyzed. The various acoustic emission statistical parameters including cumulative event, frequency distribution, amplitude distribution, and *b*-value were used for the analysis. The general fracture process is similar for all normal and crumb rubber concretes and can be divided into three distinct stages of micro-crack activity, namely, early stage, main collapse stage, and post-fracture stage. The following conclusions were drawn from the analysis: (1) more micro-cracks initiated and grew at early stage in the normal concrete, while less micro-cracks in the crumb rubber concrete but with longer stage duration; (2) the duration and crack number are both increasing with the increase in the rubber contents in main collapse and post-fracture stages; (3) new crack types associated with the rubber particles were recorded due to the change of the peak frequencies; and (4) the amplitude of the cracks decrease with the increase in the rubber content due to the damping ratio and interface improvement by the mixed rubbers. The results obtained in this article demonstrate that the acoustic emission technique can provide valuable information for a better understanding of micro-cracking and fracture monitoring of crumb rubber concrete.

Keywords

Crumb rubber concrete, acoustic emission, micro-cracking monitoring, fracture evaluation, amplitude and frequency

Introduction

Crumb rubber concrete, also called recycled tire rubber–filled concrete, is becoming a new interesting environmental material in the last two decades. More than 1.5 billion tires are produced worldwide per year, and most of these tires will sooner or later become waste.[1] Stockpiling is dangerous, not only due to a potential negative environmental impact but also because it presents a fire hazard and provides a breeding ground for rats, mice, vermin, and mosquitoes.[2–6] Management and disposal of waste tire is a major environmental concern in many countries and is becoming a significant environmental, health, and esthetic problem that is not easily solved. The use of waste tires as a concrete additive is a possible disposal solution.[5,7] Modification of concrete properties by the addition of appropriate materials is a popular field of concrete research. The brittle nature of concrete and its low loading toughness compared to other materials have prompted the use of waste tire particles as a concrete aggregate to possibly remedy or reduce these negative attributes.[8] As a combination of concrete and rubber particles, crumb rubber concrete can not only efficiently improve mechanical properties of the concrete

[1]Key Laboratory of Coast Civil Structure and Safety of Ministry of Education/School of Civil Engineering, Tianjin University, Tianjin, China
[2]Department of Structural, Geotechnical and Building Engineering, Politecnico di Torino, Torino, Italy

Corresponding author:
Qinghua Han, Key Laboratory of Coast Civil Structure and Safety of Ministry of Education, School of Civil Engineering, Tianjin University, Tianjin 300072, China.
Email: qhhan@tju.edu.cn

but also ease the potential environment threat as an alternative for waste tire recycling.

The importance of recycling of waste tires coupled with the interest in overcoming the aforementioned concrete defects has motivated a significant body of research related to crumb rubber concrete. Different kinds of tests with different volumetric fractions were conducted to investigate the static, dynamic, and fatigue mechanical behaviors of crumb rubber concrete.[2–4,7,8] During the 1990s, Topçu[9] pioneered the study of the mechanical properties of crumb rubber concrete and reported the ductility increase and applications where energy absorption capacity was required and high strength was not necessary. Li et al.[10] studied the properties of two crumb rubber mixes with same replacement ratio but different pre-saturated treatments of rubber particles and found that the crumb rubber concrete with the cement paste pre-saturated rubber particles presented the best mechanical performance, especially concerning compressive strength. Khatib and Bayomy[11] studied rubberized Portland cement concrete and offered some practical uses of crumb rubber concrete, including reduction factors. Zheng et al.[12] concluded that the incorporation of rubber particles in concrete not only decreased the natural frequency of a structural element but also led to an increase in the damping ratio. Besides the good static and dynamic behaviors, crumb rubber concrete is widely used in road pavements and other applications since the first pavement made of crumb rubber concrete had been built in Arizona State University in 1999.[13,14] Tests conducted by Hernandez-Olivares and Barluenga[15] found that crumbed tire rubber additions in structural concrete slabs could improve the fire resistance and driving comfortableness. Han et al.[16] showed that crumb rubber blends might present a potentially viable alternative to current concrete highway noise barriers due to its good noise reduction. Recently, the crumb rubber concrete was employed into the composite structures, such as steel–concrete composite beams, and found that the fatigue behaviors were greatly improved with the help of the crumb rubber concrete.[17]

In spite of extensive work done on the mechanical properties of crumb rubber concrete, the experimental work aimed at understanding of precursory microcracking and physical processes that are responsible for the fracture behavior or monitoring is relatively less.[18] Even if researchers working in concrete engineering are able to predict failure loads, it is essential to understand the relation between nucleation of cracks, crack growth, crack bridging, friction between two cracked surfaces, and the corresponding effects on the macroscopic behavior and fracture of concrete. It logically follows that to formulate predictive models for large-scale structural performance and reliability, and it is essential to understand the micro-structure performance relationships. It is vital to study how the micro-cracks and macrocracks are generated under loading for ensuring the reliability of the concrete structure.[19] The study of micro-cracking and fracture properties in crumb rubber concrete is an important topic to be able to fairly comment on the integrity of the structure. In this connection, the acoustic emission (AE), which are generated during the various stages of micro-cracking and fracture, if detected and analyzed, can lead to many advantages. It became possible because of the fact that the number of AE events is more or less proportional to the number of growing cracks, and the AE amplitudes (or energy) are proportional to the length of the crack growth increments in materials such as concrete and rock.[20–22] Compared with other monitoring techniques, the AE technique is useful to detect and monitor the formation of micro-cracks and their growth during the entire fracturing process in quasi-brittle materials.[23–29] In recent years, the application of high-speed multi-channel AE waveform recording and source location systems have led to many significant advances in the study of fracture process in concrete, rock, and other quasi-brittle materials.[29] The statistical data of AE parameters have been utilized for studying the evolution of pre-failure microcracking, precursory sequences, and fracture process in concrete and rocks. In fact, research in the field of AE testing of concrete structures and analytical and interpretation methods of AE are undergoing a drastic improvement due to increasing need for the health monitoring and renovation of concrete structures.[27] Rigorous research work has led to the realization of some practical applications of AE testing. Several researchers have applied the AE technique for the detection, characterization, evaluation, and assessment of damage in concrete structures using both signal-based and parametric-based techniques.[30–32]

In this study, the fracture processes of crumb rubber concrete with three rubber content levels (0%, 10%, and 15%) was investigated using AE techniques through axial compression tests. AE signals emitted from the concrete fracture process were acquired during the compression test. Conventional AE parameters, cumulative AE event, frequency distribution, amplitude distribution, and *Ib*-value analysis were then used to reveal the characteristics of the fracture processes of crumb rubber concrete. This work is just a beginning to come out with standard monographs to classify the damage of the crumb rubber concrete and crumb rubber concrete structures in terms of AE statistical parameters with respect to time.

Experimental procedure

Raw materials and mix proportions

The raw materials used for test concretes are fine aggregate, coarse aggregate, water, and crumb rubber within 1- to 2-mm diameters. Besides, the high-range water-reducing admixture is adopted to insure the high fluidity of concrete mixing. The mix proportions of crumb rubber follow the principle of volume percentage method, and the rubber content is divided into three groups 0% (normal concrete), 10% (100 kg/m^3), and 15% (150 kg/m^3).[17] These three groups of concrete were designed to be the same grade level of C30. The optimal mix proportions of the components were achieved by testing 37 group trials on crumb rubber concrete and the detailed results are listed in Table 1. Nine prism blocks with a size 100 mm × 100 mm × 300 mm were designed and fabricated, and there are three same specimens for each rubber content groups. The 28-day compressive strength of cubic concrete according to the test methods of building material properties are listed in Table 1.[33] The specimens were curing in the standard curing room (temperature is 20°C ± 3°C and relative humidity is above 90%) for the first 28 days and then under the condition of room temperature.

Table 1. Details of the concrete mixture proportions.

Property	0%	10%	15%
Crumb rubber (kg/m^3)	0	100	150
Cement (kg/m^3)	295	590	590
Coarse aggregate (kg/m^3)	1087	1230	1230
Fine aggregate (kg/m^3)	839	412	412
Water (kg/m^3)	165	168	168
Water reducing (kg/m^3)	2.17	6.52	7.39
Compressive strength, MPa (28 days)	43.30	43.70	35.13

Test setup

The test setup consisted of loading system and AE monitoring system. A testing machine of 5000-kN capacity with a servo-controlled hydraulic loading frame was adopted to apply load on the prismatic concrete samples in the compression testing. On the two surfaces of the concrete sample, the measuring points of longitudinal strain were arranged at the center of the trisection. Two electronic extensometers were used to measure the mid-height strain of the sample and the details are shown in Figure 1. During the test, the force control loading scheme with a loading rate of 1.5 kN/s before the peak load was first adopted and then a displacement control loading scheme was applied at a rate of 10×10^{-6} until the concrete specimen was crushed.

The AE monitoring system consisted two AE sensors and a PC-based multi-channel monitoring system sensor-based acoustic multi-channel operating system (SAMOS) AE^{win} manufactured by Physical Acoustic Corporation (PAC).[34] Appropriate AE sensor types are important in the fracture monitoring of concrete structures. Since concrete is known to be a highly attenuating material, lower frequency sensors are suitable for AE studies. Accordingly, one R6A with highest sensitivity between 35 and 100 kHz is selected for monitoring the highly attenuating concretes. However, the maximum aggregate size in concrete for this study is 20 mm, and 3500 m/s was normally used as sound velocity in concrete. Using the relation $V = n\lambda$, the frequency of the AE sensor to be used is desirable to be less than 180 kHz, and this frequency is within the range of 100–500 kHz. Considering this point, another R15A with highest sensitivity between 50 and 400 kHz was also selected in the test. The R6A and R15A together constructed the sensor monitoring system. The gains of the preamplifiers and the acquisition system were set to 20 and 40 dB, respectively. The acquisition threshold was set to 40 dB to ensure a high signal-to-noise ratio to avoid background noise. Vacuum grease LR (high-vacuum silicon grease) was used as a coupling agent to fix the sensors on the opposite surfaces of the concrete, as shown in Figure 1. The band-pass analog filter was set to between 20 kHz and 2 MHz, and the sampling frequency was set to 10 MHz.

Test results and discussion

Test phenomena

During the loading process, tiny cracks first appeared at the top of all specimens, and the crack propagated downward gradually. The more rubbers mixed in the concrete samples, the slower the tiny crack appeared and developed. When reaching bearing capacity, fragments from the ordinary concrete instantaneously ruptured, and the rupture was accompanied with a loud noise. Then, the load quickly dropped. However, there were less-ruptured fragments for the crumb rubber concrete, and the process of damage and unloading took more time. The final collapsed conditions are shown in Figure 2, and the mechanical properties are listed in Table 2, where the ultimate strain is defined as the strain value when the ultimate load dropped 15%.

Figure 2 shows the typical damaged situation of prismatic concrete samples with different rubber contents very significantly. There is one fatal penetrating crack on the surface when the crumb rubber content is 0% in Figure 2(a), and the top of the sample is badly damaged. When there is 10% rubber mixed in the concrete,

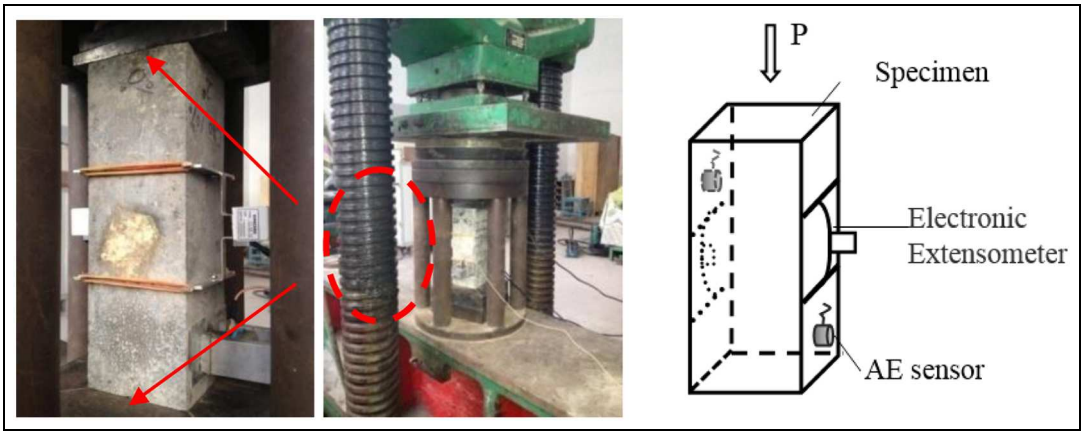

Figure 1. Setup of compression test and schematic locations of measurement device.

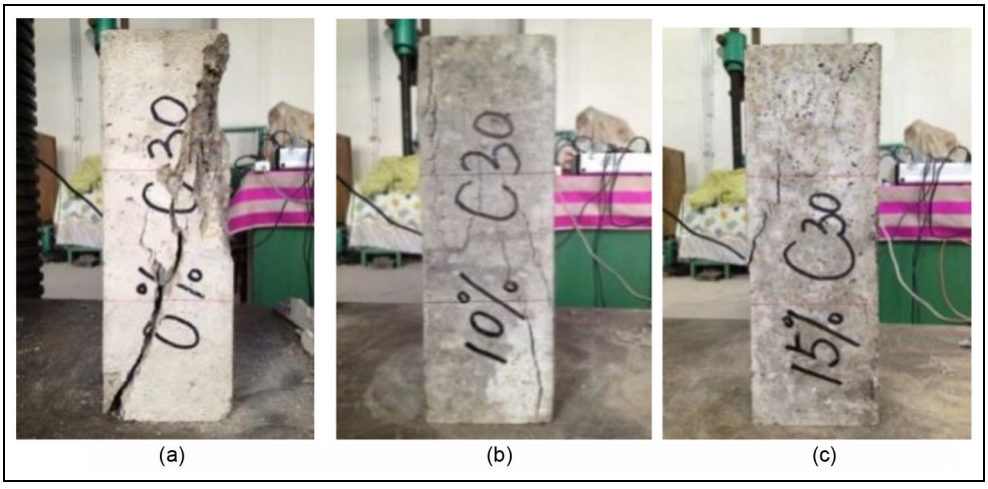

Figure 2. Typical damaged situation of prism specimens: (a) 0%, (b) 10%, and (c) 15%.

Table 2. The ultimate stress and strain of concrete with different rubber contents.

Rubber content (%)	Ultimate load (kN)	Ultimate strength (MPa)	Peak strain	Ultimate strain
0	34.063	34.063	0.002725	0.003516
10	33.471	33.471	0.004323	0.006943
15	29.412	29.412	0.004472	0.007104

there are multiple cracks rather than just one fatal penetrating crack as shown in Figure 2(b) and the concrete sample maintains integrity with four relatively long cracks, uniformly distributed on the surface. The condition of the concrete sample is even better when the rubber content is 15%, as shown in Figure 2(c).

As shown in Figure 3, compared with the ordinary concrete, the increasing ranges of peak strain in the crumb rubber concrete with 10% and 15% rubber content are 60% and 65%, respectively, and ultimate strain are 97% and 102%, respectively. Moreover, the descent stage of the stress–strain curve becomes more gradual, which proves the crumb rubber concrete has superior plasticity and ductility properties.

AE evaluation of fracture process

From the aforementioned test results, although we can observe the macrocrack conditions of the concretes during the compression test and get the superior

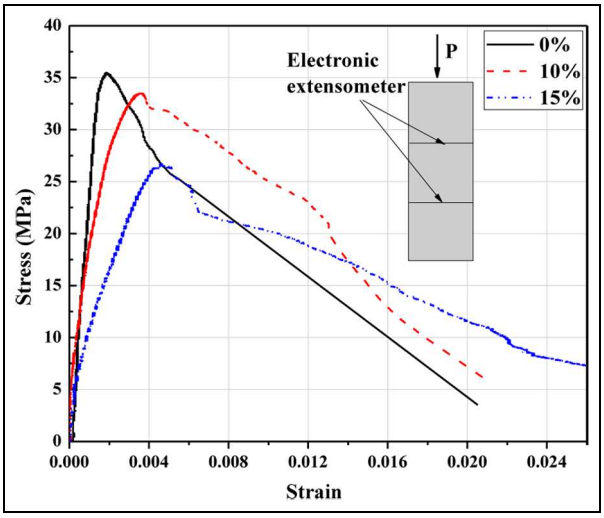

Figure 3. Stress–strain curve of concretes with different rubber contents.

plasticity and ductility properties of crumb rubber concrete, the micro-cracking activity is still unclear for us. In this part, the micro-cracking activity and fracture evaluation will be revealed by the AE analysis. The recorded AE data files were replayed and analyzed using the AE^{win} software for the identification and evaluation of various stages of fracture process using the AE statistical parameters.

Brief introduction of AE parameters. Common AE characteristic parameters are shown in Figure 4 and include rise time, duration time, count, amplitude, and energy. One AE waveform corresponds to one AE event. The energy of a waveform is the area above the threshold and below the envelope curve of the waveform. The AE peak frequency is defined as the point corresponding to the peak value on the power spectrum of a waveform.

The origin and development of micro-cracking activity in concrete can be inferred from AE statistics, as the number of AE events is more or less proportional to the number of growing cracks and the AE amplitude or energy count data are proportional to the crack growth increments in brittle and quasi-brittle materials like rock and concrete.[19,35] In fact, the formation of microcracks is ubiquitous in brittle and quasi-brittle materials at stresses close to the yielding point. The useful AE statistical parameters to identify and characterize the various stages of micro-cracking activity in concrete are as follows: AE events and cumulative of AE events, amplitude distribution, frequency distribution, and *b*-value as detailed in the following sections.

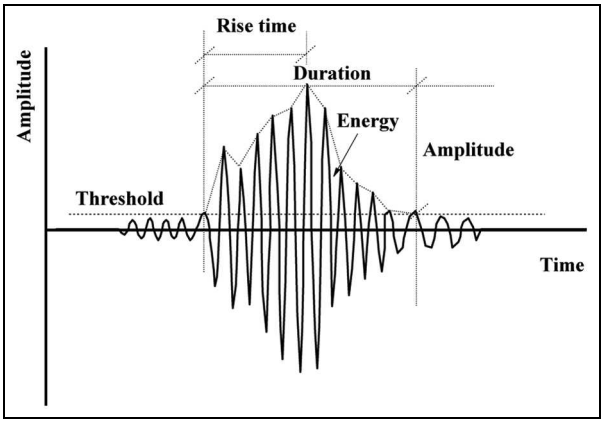

Figure 4. Traditional AE parameters.

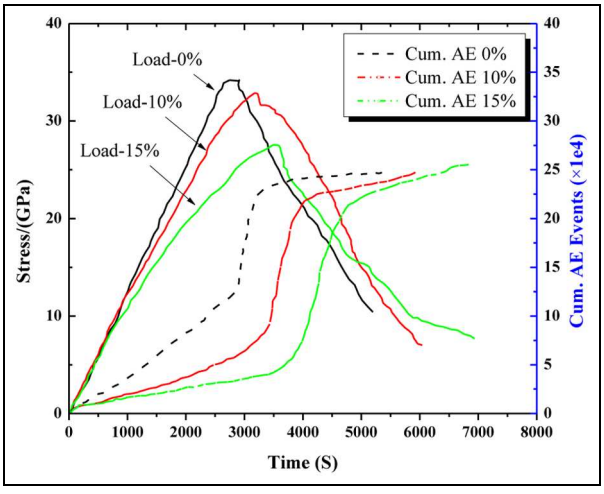

Figure 5. Plot of load and cumulative AE event versus time.

Load–time curve and cumulative of AE events. The typical curves of recorded load and cumulative of AE events versus time are identified in Figure 5 to study the variation of AE events with loading time in concrete specimen.

Figure 5 shows the general conditions of cumulative of AE events, which means the number of received signals changing with load are more or less similar for the three groups. We can observe that the curve related to the cumulative AE events versus time plot initially starts with less slop, then the slop becomes steeper as the load reaches the maximum, and then the slop gradually decreases. The results of this study show that micro-cracking activity occurs in three successive stages, namely, early stage (I), main collapse stage (II), and post-fracture stage (III). Stage-I is the initiation stage showing the micro-cracking condition before the

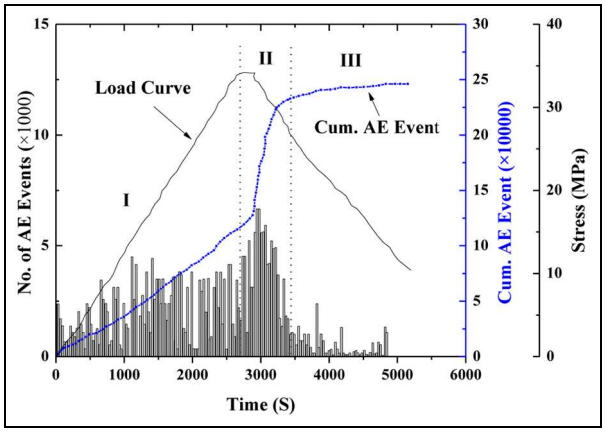

Figure 6. AE events during the compression test for concrete with 0% rubber content.

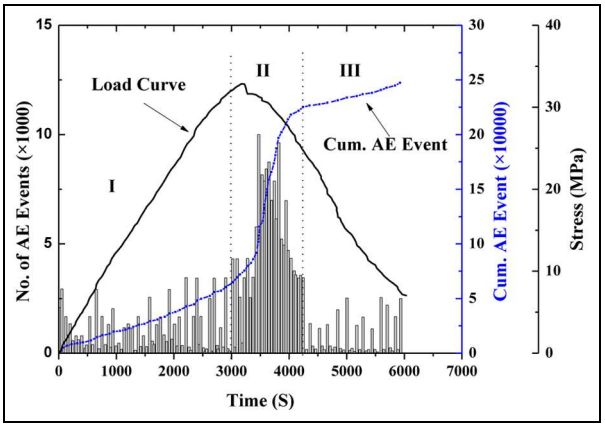

Figure 7. AE events during the compression test for concrete with 10% rubber content.

main collapse, Stage-II is the main collapse stage when the main fracture happens in the concrete, and Stage-III is the post-fracture stage which shows crack activity after the main fractures. The statistics of AE during these stages are distinctly different for the three groups as detailed in Figures 6–8.

As shown in Figures 6–8, fluctuations in the AE events can be observed during the loading processes, and these fluctuations are caused by the nonuniformity of the fracture processes of concrete and crumb rubber concrete, which is due to the complexity of concretes. An obvious increase in the number of AE events can be attributed to a larger fracture in concrete.

Stage-I starts from the beginning of the test to the peak or pre-peak load, and the micro-crack occurs and accumulates in this stage. With the increase in the rubber content from 0%, 10% to 15%, the duration of this stage increases from 2700, 3000 to 3500 s. However, if we check the slope of the cumulative AE events in Figure 5, we can find that the slope decreases. This means the less micro-cracks happen in a longer duration. From this point, we can know that the micro-crack occurs less in this stage when the rubber contents increase due to contribution of the rubber making the concrete more "elastic." This fact is proved again by the AE events in Figures 6–8, from which we can observe that AE events decreases with the increase in the rubber contents.

Stage-II is the macrocrack or main collapse stage, which is the critical stage for the concrete specimens as well as the concrete structures. First, we can see that the slope of the cumulative AE events is becoming more gradual with the increase in the rubber contents, and this indicates that the concrete is becoming more ductile. Second, with the increase in the rubber content from 0%, 10% to 15%, the duration of this stage

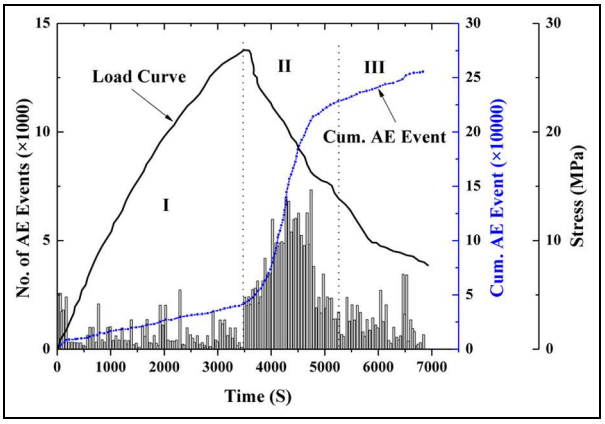

Figure 8. AE events during the compression test for concrete with 15% rubber content.

increases from 800, 1200 to 1700 s. The recorded AE events in this stage also increases with the increase in the rubber contents. This can reflect that the more cracks happen in longer duration, which is good for the samples or actual structures.

Stage-III is the post stage after the main collapse, and the main observation is that there are less AE events recorded for the normal concrete, while there are still lots of AE events can be recorded for the concrete with 15% rubber content. This means that the concrete sample is fully broken in the Stage-II, and there is little strength storage for the normal concrete, which is why we define the concrete as a brittle material. Whereas the brittle condition is gradually improved with the increase in the mixed rubber and there is still strength storage for the crumb rubber concrete after the main collapse. This is coincidence with the failure conditions of the specimens shown in Figure 2.

Frequency distribution of AE events. Previous studies indicate that the peak frequencies of AE signals generated from concrete are below 300 kHz.[20,36,37] Corresponding to different failure modes of concrete, the peak frequencies are different and utilized to recognize the failure patterns.[38–42] For normal concrete, AE sources include the expansion of inherent micro-cracks, cracking of mortar and aggregate, friction, and debonding on the surface between the aggregate and mortar. For crumb rubber concrete, additional AE sources may come from the debonding on the surface with the rubber particles.

The peak frequencies of the concretes are shown in Figure 9. For the normal concrete specimen, the distribution of peak frequencies has two main bands, including 25–55 kHz and 129–160 kHz. A small number of AE events are found between 55 and 129 kHz and 160 and 300 kHz. For the 10% rubberized concrete specimen, the distribution of peak frequencies also has two main bands, including 27–55 kHz and 125–165 kHz (a little wider than that of normal concrete). In the 10% rubberized concrete specimen, more AE events are found between 55 and 125 kHz and 165 and 300 kHz comparing to the normal specimen. These AE events are generated from concrete, rubber cracking, rubber-matrix debonding, and so on. The distribution of frequency for the 15% rubberized concrete specimen is similar with that of the 10% rubberized concrete specimen, in additional to the two similar main bands, including 27–55 kHz and 125–165 kHz, the distribution of the frequency between 75 and 100 kHz is more obvious.

Due to the complexity of AE sources and characteristics of wave propagation, successful distinction of these AE sources is difficult. However, we can still find some interesting results that the frequency between 55 and 100 kHz is increasing with the increase in the rubber contents. These AE events are generated from concrete, rubber cracking, and rubberized debonding cracks based on the previous peak frequency analysis.

Amplitude distribution of AE events. As shown in Figure 10, the points show the amplitude distribution of AE events with loading history, and we can know that the amplitudes of AE events also change with the increase in the rubber contents in the three different stages. The amplitude in the normal concrete is generally greater than that in the two crumb rubber concrete in the three stages. In the early stage, most of the events with amplitudes are less than 80 dB for normal concrete, whereas the corresponding values are about 70 and 60 dB for the two crumb rubber concrete. The similar conclusion can be obtained in the post-fracture stage that the corresponding amplitude becomes smaller with the increase in rubber particles, although the number of the events show an inverse property. For the main collapse stage, the high amplitude appears for both normal concrete and crumb rubber concrete.

The amplitude decrease can be due to different reasons, for example, due to the attenuation of the AE events. Ultrasonic attenuation from AE source to the sensor (receiver) could reduce the measured AE amplitude. The reasons for the changes in amplitude in addition to the compositional and preparation differences could be many. This could be due to strong interfaces between coarse aggregates and cement mortar. The concrete specimens contains micro-silica, which reduces porosity at the cement–aggregate interface. This interface plays an important role in both fracture properties and AE properties. Stronger interfaces generally lead to higher strength but also higher brittleness (through a smaller fracture process zone). The stronger interfaces also may likely alter the AE activity by leading to fewer AE events but more energy release per AE event. Thus, in this study, authors' opinion is that the mixed rubber changes the original strong interface to be less strong. In addition, the energy loss experienced by these stress waves per unit distance travel will be related to the damping capacity (internal friction) of the material. This also causes the reduction of the total elastic wave energy that reaches the sensor. In this case, it is reasonable for us to conclude that the mixed rubber particles improve the damping ratio of the concrete and the attenuation decreases more.

b-value analysis

In spite of existence of breaks in earthquake scaling caused by temporal and spatial heterogeneity, the assumption of self-similarity of the earthquake process is found in most cases.[43] In earthquake seismology, larger magnitude earthquakes occur less frequently than ones of smaller magnitude. Self-similarity is consistent with the observed linear *b*-value relation of the Gutenberg–Richter (GR) law[44]

$$\log_{10} N(M) = a - bM \tag{1}$$

where $N(M)$ is the number of events with magnitude equal to or greater than M, and a and b are real constants that may vary in space and time. The significance of the b parameter for quantifying seismicity or for earthquake prediction has been recognized widely by seismologists.[45,46]

Because AEs and earthquakes have similar mechanisms, this method can also be applied to the AE field. The principle is that micro-cracks release more AE events with smaller amplitude, while macrocracks release fewer AE events with larger

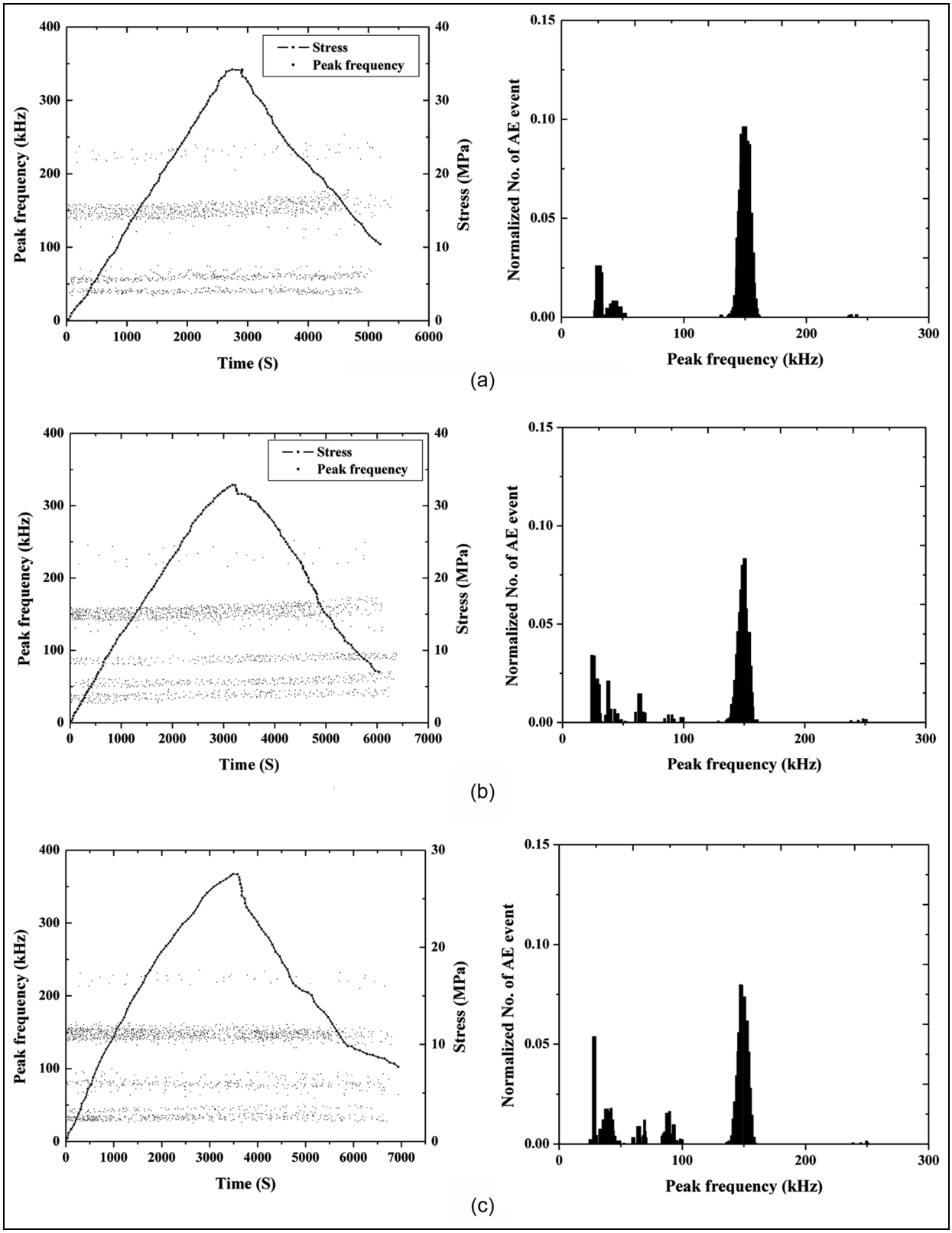

Figure 9. Distribution characteristics of peak frequencies for concrete with different rubber contents: (a) concrete with 0% rubber content, (b) concrete with 10% rubber content, and (c) concrete with 15% rubber content.

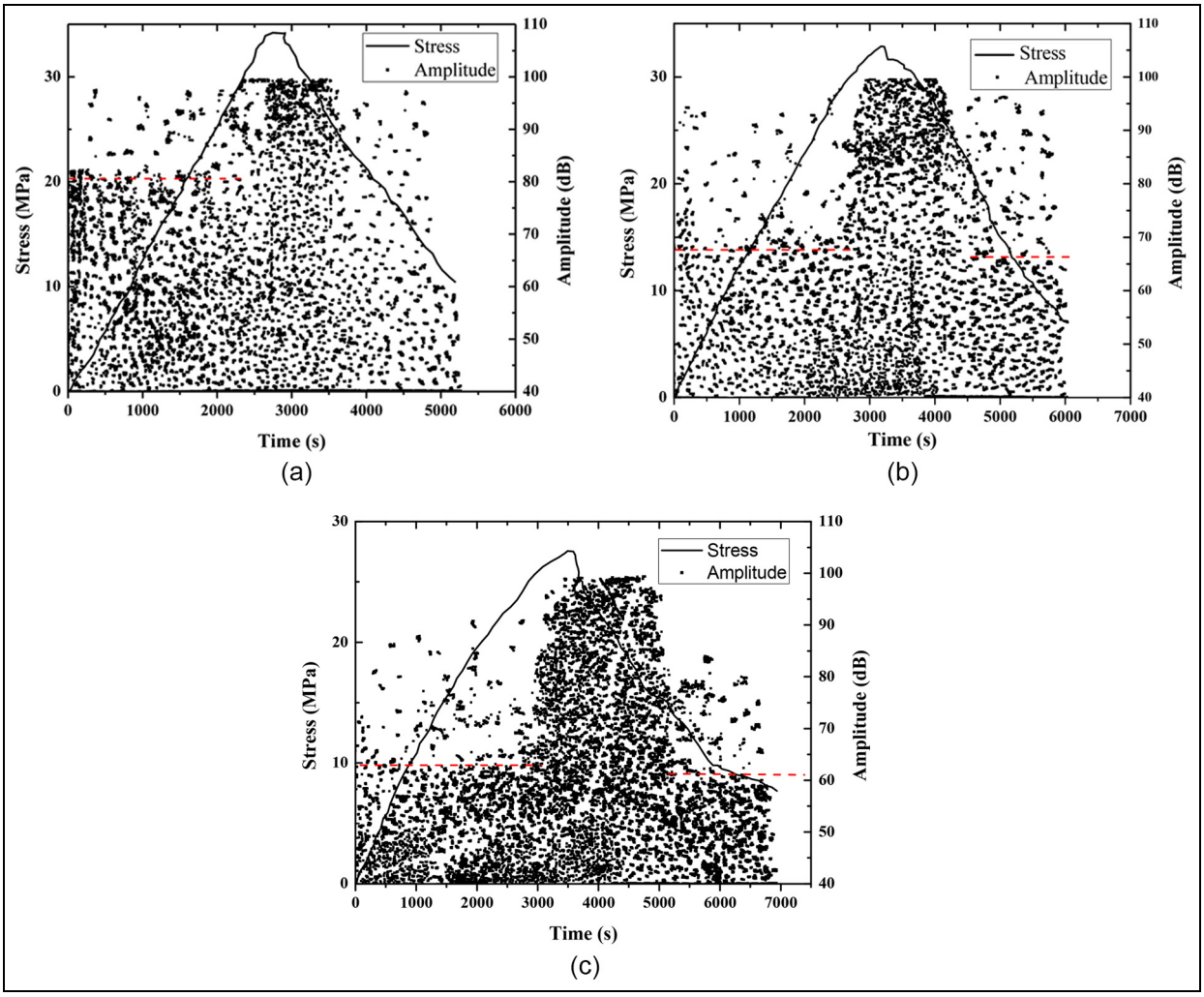

Figure 10. Amplitude of AE during the fracture process: (a) rubber content—0%, (b) rubber content—10%, and (c) rubber content—15%.

amplitude. Equation (1) can be changed to the following form[21,31,47]

$$\log_{10}N = a - b'\left(\frac{A_{dB}}{20}\right) \tag{2}$$

where N is the number of AE events with magnitudes greater than A_{dB}; A_{dB} is peak amplitude of the AE events in decibels; and b' is slope of regression line of plot of $\log_{10}N$ against A_{dB}, also called the b-value of these AE events. From equation (2), when micro-cracks (rather than macrocracks) are dominant in a fracture process A, a bigger b' value is obtained; when macro-cracks (rather than micro-cracks) are dominant in a fracture process B, then a smaller b' value is obtained. To account for the statistical characteristics of the amplitude distributions of AE events, Shiotani et al.[48,49] proposed the Ib-value method using the statistical information of AE events. The Ib-value is defined by the following equation

$$Ib = \frac{\log_{10}N(\mu - \alpha_1\sigma) - \log_{10}N(\mu + \alpha_2\sigma)}{(\alpha_1 + \alpha_2)\sigma} \tag{3}$$

where σ and μ are standard deviation and mean value of amplitude distribution of AE event group, respectively; α_1 and α_2 are coefficients related to the AE event group; $N(\mu - \alpha_1\sigma)$ is number of AE events with amplitude larger than $\mu - \alpha_1\sigma$; and $N(\mu + \alpha_1\sigma)$ is number of AE events with an amplitude larger than $\mu + \alpha_1\sigma$. The values of α_1 and α_2 are dependent on the statistical characteristics of the amplitude distributions of the AE events. The methodology for calculating α_1 and α_2 can be found in Shiotani et al.[48]

The Ib-value analysis is determined to be feasible for monitoring slope failure, evaluation of rock fracture

processes, and damage assessment of reinforced concrete (RC) beams and RC beams strengthened with fiber-reinforced plastic (FRP).[50] However, little research has been conducted on applying *Ib*-value analysis to the monitoring of fracture processes of crumb rubber concrete. During the experiment, AE amplitude data were acquired with the help of AE^{win} PAC system and stored. The *Ib*-value methods as a function of time are used in the fracture process analysis and on the assessment of its potential as a fracture precursor based on the recorded data analyzed using MATLAB.

To study variations of *Ib*-value with time, a sliding time-window method is used, instead of the previous sliding event-window.[51] The *Ib*-value is calculated for the first T events. Then, the window is shifted by a time, for example, $T/10$ events. The *Ib*-value is calculated for the new group of data, and the process is repeated until the last event is reached. Every calculated *Ib*-value is assigned to the middle time of the corresponding window.

The *Ib*-value curves of the normal concrete and crumb rubber concrete specimens are shown together with loading curves and AE amplitudes in Figure 10. At early stage, the *Ib*-value shows an increasing trend in value with the increase in the rubber contents. This phenomenon can be explained that the fracture magnitude in the crumb rubber concrete is smaller than that in the normal concrete, and the corresponding *Ib*-value is relatively bigger in the crumb rubber concrete. Therefore, *Ib*-value can reveal the difference in the fracture process between the normal concrete and the crumb rubber concrete at the early stage. From Figure 10(a)–(c), there is an obvious decrease in the *Ib*-values around the start of the mainly collapse stage, revealing that the fracture patterns shifted from micro-cracks to macrocracks. The *Ib*-values fluctuate in local regions because the complexity of concretes causes a nonuniform fracture process. The *Ib*-value of 1.5 can be taken as an alarm value to suggest people to pay attention to the specimen or the real structures.

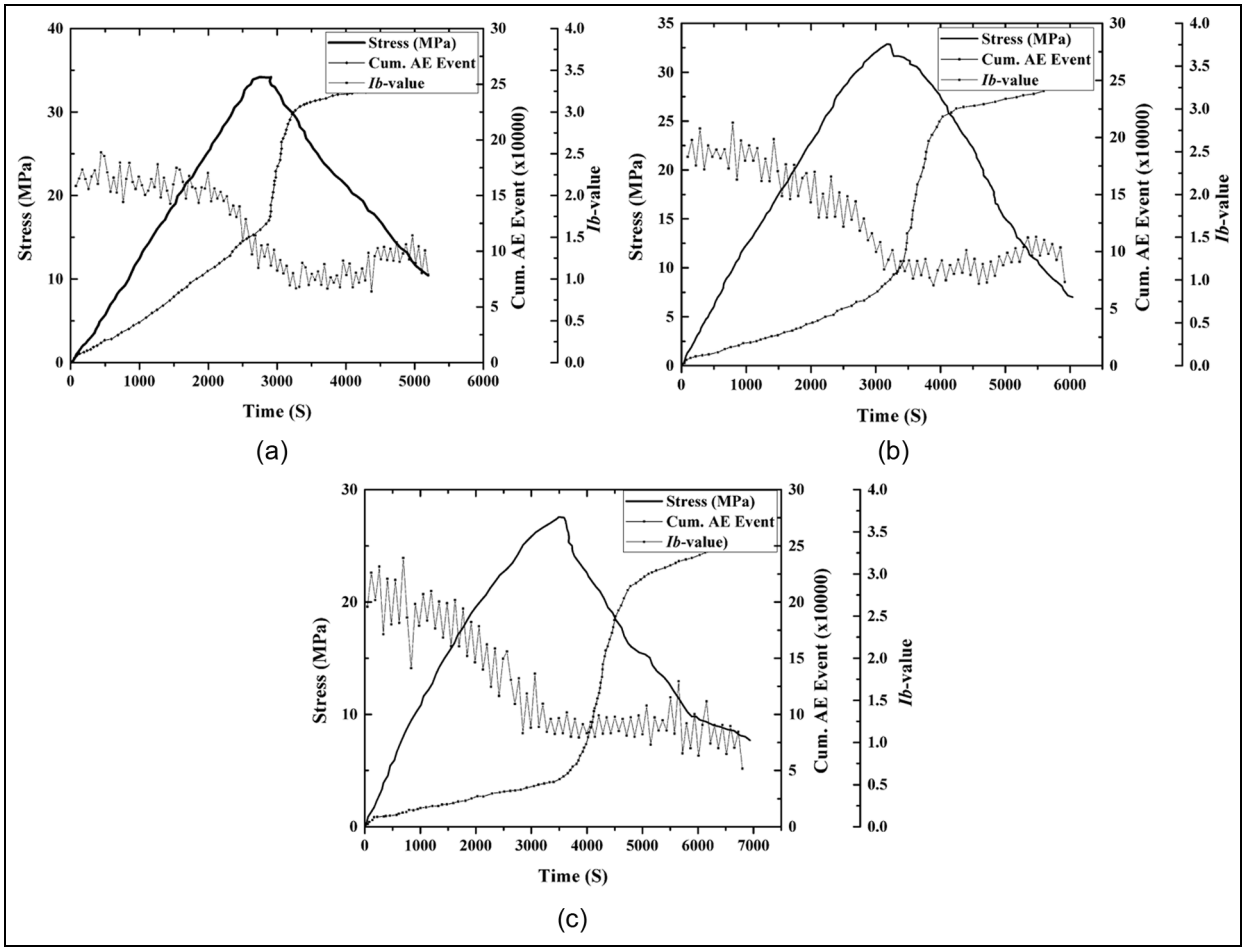

Figure 11. *Ib*-value and slope of cumulative AE event as the fracture precursor: (a) rubber content—0%, (b) rubber content—10%, and (c) rubber content—15%.

Considering that the slope of the cumulative AE events increase sharply when the fracture process enters into the main collapse, the slope of the cumulative AE events can also be taken as the precursor of the failure. Thus, we combine the *Ib*-value and the slope of the cumulative AE events together to give double check for the precursor of the failure or the dangerous condition, as shown in Figure 11. It is obvious to see that when the *Ib*-value is smaller than 1.5, the slope of the cumulative AE events also start to increase sharply compared to the former stage. Similar phenomena can be observed for all the three concretes. In this case, it is reasonable to take the *Ib*-value and the slope of the cumulative AE events as the double check precursor of the failure.

Conclusion

AE technique was successfully applied in the crack monitoring on the crumb rubber concrete during the fracture test. The results obtained in the laboratory are useful to understand the various stages of the micro-cracking activities during the fracture process for the normal concrete and the crumb rubber concrete. Based on the above results, the following major conclusions can be drawn:

1. The parametric analysis of AE has revealed that micro-cracking occurs in three distinct and successive stages, namely, early stage, main collapse stage, and post-fracture stage in both concrete and crumb rubber concrete specimens.
2. Both concrete and crumb rubber test specimens have shown similar trends with regard to the cumulative AE events versus time. We can observe that the curve related to cumulative AE events versus time plot initially starts with less slope, then the slope becomes steeper as the load reaches the maximum, and then gradually the slope decreases. The results have helped in identifying the crack initiation and crack damage states for the tested samples.
3. Compared with the normal concrete, the duration of the early stage is increasing with the increase in the mixed rubber content, and the number of cracks is decreasing. This can reveal the fact that the elastic property of the concrete is improved by the rubber particles and it needs more time for the same deformation.
4. The duration and number of cracks both increase as the rubber particles increase and reveal that the concrete is becoming less brittle in the collapse stage and more cracks with less amplitude happens, which is good for the actual application due to the energy absorption capacity from the dangerous structures.
5. More cracks associated with rubber particles are recorded during the fracture process with relative low frequency, and the amplitude of the cracks is decreased due to the damping ratio improvement by the rubber particles.

Declaration of conflicting interests

The author(s) declared no potential conflicts of interest with respect to the research, authorship, and/or publication of this article.

Funding

The author(s) disclosed receipt of the following financial support for the research, authorship and/or publication of this article: This work was supported by the National Natural Science Foundation of China (Nos 51408408 and 51525803), Tianjin Natural Science Foundation (No. 16JCQNJC07400), and Science and Technology Project of MOHURD (No. 2016K3004).

References

1. Karakurt C. Microstructure properties of waste tire rubber composites: an overview. *J Mater Cycles Waste* 2015; 17: 422–433.
2. Eldin NN and Senouci AB. Measurement and prediction of the strength of rubberized concrete. *Cement Concrete Comp* 1994; 16: 287–298.
3. Toutanji HA. The use of rubber tire particles in concrete to replace mineral aggregates. *Cement Concrete Comp* 1996; 18: 135–139.
4. Fedroff D, Ahmad S and Savas BZ. *Mechanical properties of concrete with ground waste tire rubber*. Transportation research, record no. 1532, 1996. Washington, DC: Transportation Research Board.
5. Ganjian E, Khorami M and Maghsoudi AA. Scrap-tyre-rubber replacement for aggregate and filler in concrete. *Constr Build Mater* 2009; 23: 1828–1836.
6. Smith R, Ferrebee E, Ouyang YF, et al. Optimal staging area locations and material recycling strategies for sustainable highway reconstruction. *Comput-Aided Civ Inf* 2014; 29: 559–571.
7. Li G, Garrick G, Eggers J, et al. Waste tire fiber modified concrete. *Compos Part B: Eng* 2004; 35: 305–312.
8. Khaloo AR, Dehestani M and Rahmatabadi P. Mechanical properties of concrete containing a high volume of tire–rubber particles. *Waste Manage* 2008; 28: 2472–2482.
9. Topçu IB. The properties of rubberized concretes. *Cement Concrete Res* 1995; 25: 304–310.
10. Li Z, Li F and Li SL. Properties of concrete incorporating rubber tyre particles. *Mag Concrete Res* 1998; 50: 297–304.
11. Khatib ZK and Bayomy FM. Rubberized Portland cement concrete. *J Mater Civil Eng* 1999; 11(3): 206–213.
12. Zheng L, Sharon HX and Yuan Y. Experimental investigation on dynamic properties of rubberized concrete. *Constr Build Mater* 2008; 22: 939–947.

13. Zhu H, Liu CS, Zhang YM, et al. Effect of crumb rubber proportion on compressive and flexural behavior of concrete. *J Tianjin Univ* 2007; 40(7): 761–765.
14. Yang LH, Zhu H and Li CF. Strengths and flexural strain of CRC specimens at low temperature. *Constr Build Mater* 2011; 25: 906–910.
15. Hernandez-Olivares F and Barluenga G. Fire performance of recycled rubber-filled high-strength concrete. *Cement Concrete Res* 2014; 34(1): 109–117.
16. Han Z, Chunsheng L, Kombe T, et al. Crumb rubber blends in noise absorption study. *Mater Struct* 2008; 41: 383–390.
17. Han QH, Wang YH, Xu J, et al. Static behavior of stud shear connectors in elastic concrete–steel composite beams. *J Constr Steel Res* 2015; 113: 115–126.
18. Landis EN and Baillon L. Experiments to relate acoustic emission energy to fracture energy of concrete. *J Eng Mech: ASCE* 2002; 128: 698–702.
19. Vidya Sagar R, Prasad RV, Raghu BK, et al. Microcracking and fracture process in cement mortar and concrete: a comparative study using acoustic emission technique. *Exp Mech* 2013; 53: 1161–1175.
20. Ohtsu M. Acoustic emission characteristics in concrete and diagnostic applications. *J Acoust Soc Am* 1987; 6(2): 99–108.
21. Colombo IS, Main IG and Forde MC. Assessing damage of reinforced concrete beam using "*b-value*" analysis of acoustic emission signals. *J Mater Civil Eng* 2003; 15(3): 280–286.
22. Rao MVMS, Prasanna LKJ, Nagaraja RGM, et al. Precursory microcracking and brittle failure of Latur basalt and migmatite gneiss under compressive loading. *Curr Sci* 2011; 101(8): 1053–1059.
23. Park HS, Lee HM, Adeli H, et al. A new approach for health monitoring of structures: terrestrial laser scanning. *Comput-Aided Civ Inf* 2007; 22(1): 19–30.
24. Huang RY, Mao IS and Lee HK. Exploring the deterioration factors of RC bridge decks: a rough set approach. *Comput-Aided Civ Inf* 2010; 25(7): 517–529.
25. Li H, Huang Y, Chen WL, et al. Estimation and warning of fatigue damage of FRP stay cables based on acoustic emission techniques and fractal theory. *Comput-Aided Civ Inf* 2011; 26: 500–512.
26. Aggelis DG. Classification of cracking mode in concrete by acoustic emission parameters. *Mech Res Commun* 2011; 38: 153–157.
27. Carpinteri A, Xu J, Lacidogna G, et al. Reliable onset time determination and source location of acoustic emissions in concrete structures. *Cement Concrete Comp* 2012; 34: 529–537.
28. Mpalaskas AC, Thanasia OV, Matikas TE, et al. Mechanical and fracture behavior of cement-based materials characterized by combined elastic wave approaches. *Constr Build Mater* 2014; 50: 649–656.
29. Han QH, Xu J, Carpinteri A, et al. Localization of acoustic emission sources in structural health monitoring of masonry bridge. *Struct Control Hlth* 2015; 22(2): 314–329.
30. Grosse CU and Ohtsu M. *Acoustic emission testing*. Berlin: Springer-Verlag, 2008.
31. Carpinteri A, Lacidogna G and Manuello A. The b-value analysis for the stability investigation of the ancient Athena Temple in Syracuse. *Strain* 2011; 47: 243–253.
32. Schumacher T, Higgins CC and Lovejoy SC. Estimating operating load conditions on reinforced concrete highway bridges with b-value analysis from acoustic emission monitoring. *Struct Health Monit* 2011; 10(1): 17–32.
33. *GB/T 50081-2002. Test methods of mechanics property of ordinary concrete*. Beijing: Chinese Industrial Standard of Building Material.
34. Physical Acoustic Corporation (PAC). *SAMOS AE system user's manual* (rev. 2). Princeton Junction, NJ: PAC, 2005.
35. Ohtsu M. The history and development of acoustic emission in concrete engineering. *Mag Concrete Res* 1996; 48: 321–330.
36. Li Z and Shah SP. Localization of microcracking in concrete under uniaxial tension. *ACI Mater J* 1994; 91(4): 372–381.
37. Wandowski T, Malinowski P, Ostachowicz W, et al. Embedded damage localization subsystem based on elastic wave propagation. *Comput-Aided Civ Inf* 2015; 30: 654–665.
38. Ramirez-Jimenez CR, Papadakis N, Reynolds N, et al. Identification of failure modes in glass/polypropylene composites by means of the primary frequency content of the acoustic emission event. *Compos Sci Technol* 2004; 64: 1819–1827.
39. Gutkin R, Green CJ, Vangrattanachai S, et al. On acoustic emission for failure investigation in CFRP: pattern recognition and peak frequency analyses. *Mech Syst Signal Pr* 2011; 25(4): 1393–1407.
40. Sause MGR, Gribov A, Unwin AR, et al. Pattern recognition approach to identify natural clusters of acoustic emission signals. *Pattern Recogn Lett* 2012; 33: 17–23.
41. Qiao L, Esmaeily A and Melhem HG. Signal pattern recognition for damage diagnosis in structures. *Comput-Aided Civ Inf* 2012; 27(9): 699–710.
42. Raich AM and Liszkai TR. Multi-objective optimization of sensor and excitation layouts for frequency response function-based structural damage identification. *Comput-Aided Civ Inf* 2012; 27(2): 95–117.
43. Han QH, Carpinteri A, Lacidogna G, et al. Fractal analysis and yule statistics for seismic prediction based on 2009 L'Aquila earthquake in Italy. *Arab J Geosci* 2015; 8(5): 2457–2465.
44. Gutenberg B and Richter CF. Frequency of earthquakes in California. *B Seismol Soc Am* 1994; 34: 185–188.
45. Smith WD. The *b*-value as an earthquake precursor. *Nature* 1981; 289: 136–139.
46. Han QH, Xu J, Carpinteri A, et al. A robust method to estimate the b-value of the magnitude–frequency distribution of earthquakes. *Chaos Soliton Fract* 2015; 81(2): 103–110.
47. Rao MVMS and Prasanna LKJ. Analysis of b-value and improved b-value of acoustic emissions accompanying rock fracture. *Curr Sci* 2005; 89: 1577–1582.

48. Shiotani T, Fujii K, Aoki T, et al. Evaluation of progressive failure using AE sources and improved b-value on slope model tests. *Prog Acoust Emission VII* 1994; 7: 529–534.
49. Shiotani T, Ohtsu M and Ikeda K. Detection and evaluation of AE waves due to rock deformation. *Constr Build Mater* 2001; 15: 235–246.
50. Yun HD, Choi WC and Seo SY. Acoustic emission activities and damage evaluation of reinforced concrete beams strengthened with CFRP sheets. *NDT&E Int* 2010; 43(7): 615–628.
51. Ma G, Li Hui and Duan ZD. Repair effects and acoustic emission technique-based fracture evaluation for predamaged concrete columns confined with fiber-reinforced polymers. *J Compos Constr* 2012; 16: 626–639.